JOURNAL OF GEOPHYSICAL RESEARCH, VOL. 113, A03S08, doi:10.1029/2007JA012558, 2008

Radiation Belt Environment model: Application to space weather nowcasting

Mei-Ching Fok,[1] Richard B. Horne,[2] Nigel P. Meredith,[2] and Sarah A. Glauert[2]

Received 23 May 2007; revised 11 September 2007; accepted 9 October 2007; published 23 January 2008.

[1] A data-driven physical model of the energetic electrons in the Earth's radiation belts, called the Radiation Belt Environment (RBE) model, has been developed to understand Earth's radiation belt dynamics and to predict the radiation conditions found there. This model calculates radiation belt electron fluxes from 10 keV to 6 MeV in the inner magnetosphere. It takes into account the realistic, time-varying magnetic field and considers effects of wave-particle interactions with whistler mode chorus waves. The storm on 23–27 October 2002 is simulated and the temporal evolutions of the radial and pitch angle distributions of energetic electrons are examined. The calculated electron fluxes agree very well with particle data from the low-orbit SAMPEX and LANL geosynchronous satellites, when the wave-particle interactions are taken into account during storm recovery. Flux increases begin near the plasmapause and then diffuse outward to higher L shells, consistent with previous findings from statistical studies. A simplified version of the RBE model is now running in real time to provide nowcasting of the radiation belt environment. With further improvements and refinements, this model will have important value in both scientific and space weather applications.

Citation: Fok, M.-C., R. B. Horne, N. P. Meredith, and S. A. Glauert (2008), Radiation Belt Environment model: Application to space weather nowcasting, *J. Geophys. Res.*, *113*, A03S08, doi:10.1029/2007JA012558.

1. Introduction

[2] The Earth's radiation belts consist of energetic electron (~100 keV to several MeV) and ions (~100 keV to several hundred MeV) trapped in the magnetosphere roughly from $1.2 < L < 8$. The energetic electrons reside in two distinct regions: the inner belt and the outer belt, which are usually separated by the slot region ($1.8 < L < 3$) of depleted particle populations. Pitch angle diffusion loss of electrons by interacting with whistler mode plasmaspheric hiss is believed to be the source of the slot region [*Lyons et al.*, 1972; *Albert*, 1994; *Meredith et al.*, 2007]. The inner belt is relatively stable while the outer belt is highly variable with geomagnetic activity. The fluxes of energetic electrons in the outer belt decrease during the main phase of a magnetic storm due to adiabatic effect [*Dessler and Karplus*, 1961; *Kim and Chan*, 1997]. Additional nonadiabatic processes also contribute to the flux decrease in the storm main phase [*Green et al.*, 2004]. During the recovery phase the flux of energetic electrons can change dramatically as well. While approximately half of all moderate and intense storms cause a net increase in the flux of energetic electrons by a factor of 2 or more, approximately a quarter of these storms result in a net decrease in the fluxes by more than a factor of 2 [*Reeves et al.*, 2003]. This variability is caused by an imbalance between acceleration, transport, and loss processes all of which become enhanced during geomagnetic storms [*Horne*, 2002; *Thorne et al.*, 2005; *Horne et al.*, 2006; *Summers et al.*, 2007]. The ratio of poststorm to prestorm flux is related to the solar wind speed [*Paulikas and Blake*, 1979; *Reeves et al.*, 2003] and the direction of the IMF B_z during the storm recovery phase [*Iles et al.*, 2002]. In some major storms the flux enhancement takes place close to the Earth and may even penetrate into the slot region [*Baker et al.*, 2004; *Zheng et al.*, 2006].

[3] The intensification of the radiation belts has significant impacts on the space environment. Moderate energy (~10 to 100 keV) electrons can cause surface charging effects and relativistic (~0.1 to 5 MeV) electrons can cause deep-dielectric charging on space systems [*Baker*, 2001]. Therefore understanding the physical processes that are controlling the development of the radiation belts during active periods and being able to predict their variability have both scientific and practical significance. Radial diffusion has traditionally been considered to be the leading transport and energization mechanism in the inner magnetosphere [*Schulz and Lanzerotti*, 1974]. However, it has recently been suggested that electrons can be accelerated efficiently by resonant wave particle interactions with whistler mode chorus waves [*Horne and Thorne*, 1998; *Summers et al.*, 1998]. Several studies have shown an association between relativistic electron flux enhancements and prolonged periods of enhanced chorus amplitudes lasting for the order of several days [*Meredith et al.*, 2002, 2003a; *Miyoshi et al.*, 2003]. Furthermore, theoretical

[1] Geospace Physics Laboratory, NASA Goddard Space Flight Center, Greenbelt, Maryland, USA.
[2] Physical Sciences Division, British Antarctic Survey, Cambridge, UK.

work suggests that the timescale for acceleration is typically of the order of 1–2 d [*Summers and Ma*, 2000; *Horne et al.*, 2005a, 2005b], consistent with observations. These studies suggest that wave acceleration by whistler mode chorus waves should be included in realistic physics-based models of the Earth's radiation environment.

[4] A number of models have been established to simulate the radiation belt dynamics and to provide interpretation for observable features. Two major approaches have been taken in modeling the radiation belts: test particle and kinetic formulations. *Li et al.* [1993] and *Hudson et al.* [1996] performed guiding center simulations of the storm sudden commencement on 24 March 1991 that was induced by an interplanetary shock. They used different models for the compressional electric fields but both studies were able to reproduce the rapid formation of a "new" electron belt at $L \sim 2.5$. *Elkington et al.* [2003] investigated the effects of ULF waves on energetic electron dynamics by tracking their guiding center motion in an asymmetric, compressed dipole field. They found outer belt electrons are accelerated and diffuse radially through drift resonance with Pc-5 ULF waves. Using a test particle approach, *Ukhorskiy et al.* [2006] simulated the evolution of outer belt electrons during the magnetic storm of 7 September 2002. They found the diamagnetic effect from the storm time ring current leads to expansion of electron drift paths that intercept with the magnetopause, producing significant irreversible loss of energetic electrons at $L > 5$ during the storm main phase.

[5] Kinetic formulation is another commonly used technique to model the radiation belt. In a kinetic model the equation of the particle distribution function is solved analytically or numerically. One simple approach is based on a standard radial diffusion equation with diffusion coefficients driven by the solar wind conditions or geomagnetic activity [*Li et al.*, 2001; *Albert et al.*, 2001]. *Varotsou et al.* [2005] and *Horne et al.* [2006] combined radial diffusion with acceleration and loss due to whistler mode chorus waves and confirmed that wave acceleration by whistler mode chorus is an important acceleration mechanism in the outer radiation belt. In particular, *Horne et al.* [2006] modeled a moderate storm due to a high-speed solar wind stream, typical of the declining phase of the solar cycle. They found that the accelerated (MeV) electrons are transported both inward and outward and increase in phase space density by a factor of 10 between $3.5 < L < 7$. For models that cover a wide range of energy, drift motion must be considered since convection is an important transport mechanism for lower-energy (<50 keV) particles [*Bourdarie et al.*, 1997; *Zheng et al.*, 2003; *Miyoshi et al.*, 2006]. Using the relativistic RAM model with dipole magnetic field, *Miyoshi et al.* [2006] simulated the dynamics of energetic electrons during the October 2001 storm. They reproduced the observed local time flux asymmetry for hot electrons (30 keV). They also concluded that only convective transport and radial diffusion cannot explain the enhancement of relativistic electrons seen during storm recovery.

[6] A convection-diffusion model, namely the Radiation Belt Environment (RBE) model, has been developed to understand the radiation belt dynamics in order to predict the flux variation during active times [*Fok et al.*, 2001, 2005; *Zheng et al.*, 2003]. The model was used to simulate a substorm injection during a dipolarization of the magnetic field [*Fok et al.*, 2001]. Observable features during substorms, such as dispersionless injection and drift echoes, are successfully reproduced. The electron flux enhancements during two magnetic storms were also studied using the RBE model [*Zheng et al.*, 2003; *Fok et al.*, 2005]. They found energization by the inductive electric field and by whistler mode waves are crucial for the flux increase during magnetic storms.

[7] The RBE model has been improved to include wave-particle interactions due to whistler mode chorus waves, to have a higher-resolution in L shell, and extended to the inner belt. In modeling the wave-particle interactions, diffusion coefficients are taken from the Pitch Angle and Energy Diffusion of Ions and Electrons (PADIE) code [*Glauert and Horne*, 2005]. In this paper, we give a brief description of the RBE formulation. We then present the RBE simulation of the storm on 23–27 October 2002. The calculated radiation belt electron fluxes are compared with observations from the Solar Anomalous and Magnetospheric Particle Explorer (SAMPEX) low-Earth orbit satellite and Los Alamos National Laboratory (LANL) geosynchronous satellites. The dynamics of the energetic electrons are discussed and the distinct roles of transport and wave acceleration are quantitatively examined. With real-time solar wind speed, density, interplanetary magnetic field (IMF), and *Dst* data as input, a simplified version of the RBE model is running simultaneously to provide now-casting of the radiation belt environment. Finally, we discuss the potentials of the RBE model for space weather applications.

2. Radiation Belt Environment Model

[8] The Radiation Belt Environment (RBE) model is a kinetic model that calculates the temporal variation of the phase space density of energetic electrons by solving the following bounce-averaged Boltzmann transport equation [*Fok et al.*, 2001; *Zheng et al.*, 2003]:

$$\frac{\partial f_s}{\partial t} + \langle \dot{\lambda}_i \rangle \frac{\partial f_s}{\partial \lambda_i} + \langle \dot{\varphi}_i \rangle \frac{\partial f_s}{\partial \varphi_i} = \frac{1}{\sqrt{M}} \frac{\partial}{\partial M} \left(\sqrt{M} D_{MM} \frac{\partial f_s}{\partial M} \right) + \frac{1}{T(y) \sin 2\alpha_o} \frac{\partial}{\partial \alpha_o} \left(T(y) \sin 2\alpha_o D_{\alpha_o \alpha_o} \frac{\partial f_s}{\partial \alpha_o} \right) - \left(\frac{f_s}{0.5\tau_b} \right)_{\text{loss cone}} \quad (1)$$

where $f_s = f_s(t, \lambda_i, \varphi_i, M, K)$, is the average distribution function on the field line between mirror points. Here λ_i and φ_i are the magnetic latitude and local time, respectively, at the ionospheric foot point of the geomagnetic field line. M is the relativistic magnetic moment and $K = J/\sqrt{8 m_o \overline{M}}$, where J is the second adiabatic invariant. The motion of the particles is described by their drifts across field lines which are labeled by their ionospheric foot points. The inner boundary of λ_i is at 11.8°, corresponding to $L = 1.06$. The outer edge of the model is bounded by field lines with λ_i at 70.2° and equatorial crossing at 10 Earth radius (R_E), whichever is closer. The M range is chosen to well represent the energy ranges of electrons from 10 keV to 6 MeV. The K range is chosen to cover the loss cone so that particle

precipitations can be estimated as well. Here α_o is the equatorial pitch angle and $y = \sin\alpha_o$. $T(y)$ is given by:

$$T(y) = \frac{1}{R_o}\int_0^{s_m} \frac{ds}{\cos\alpha} \tag{2}$$

where R_o is the radial distance in R_E of the field line equatorial crossing. The integration is along the field line from the equator to the mirror point. Here τ_b is the particle bounce period.

[9] The left-hand side of (1) represents the drifts of the particle population, and the terms on the right-hand side of (1) refer to diffusion and loss. The calculation of the bounce-averaged drift velocities, $\langle\dot{\lambda}_i\rangle$ and $\langle\dot{\varphi}_i\rangle$, were described in detail by *Fok and Moore* [1997]. These drifts include gradient and curvature drift and $\mathbf{E} \times \mathbf{B}$ drift from convection and corotation electric fields. The effects of inductive electric field due to time-varying magnetic field are also taken into account implicitly in the model. For this purpose we have assumed that field lines are rooted at the ionosphere so that the inductive electric field there is zero. However, the shapes of field lines at higher altitudes vary as a function of time according to the magnetic field model. If field lines are perfect conductors, the field line motion at high altitudes, for example, at the equator, will generate an induction electric field of the form,

$$\mathbf{E}_{\text{ind}} = -\mathbf{v}_o \times \mathbf{B}_o \tag{3}$$

where $\mathbf{v}_o$ and $\mathbf{B}_o$ are the field line velocity and magnetic field at the equator.

[10] The first term on the right-hand side of (1) represents particle diffusion in M as a result of energy diffusion due to interactions with plasma waves. The relation between the energy diffusion coefficient (D_{EE}) and the corresponding coefficient in M (D_{MM}) is given as

$$D_{MM} = D_{EE}\left(\frac{\partial M}{\partial E}\right)^2 = D_{EE}\left(\frac{E_o + E}{E_o B_m}\right)^2 \tag{4}$$

where E_o is the electron rest energy and B_m is the magnetic field at the mirror point. The second term on the right-hand side of (1) represents pitch angle diffusion from interactions with plasma waves. For pure pitch angle diffusion (E unchanged) in the (M, K) coordinates, we first map the particle phase space density from the (M, K) to (E, α_o) coordinates, perform diffusion in α_o, and then map the updated distribution back to the (M, K) coordinates [*Fok et al.*, 1996]. The diffusion terms are followed by the loss term of the loss cone, the boundary of which is assumed to correspond to mirror height of 120 km. Particles in the loss cone are assumed to have a lifetime of one half bounce period (0.5 τ_b).

[11] In this work, the bounce-averaged pitch angle and energy diffusion coefficients, $D_{\alpha_o\alpha_o}$ and D_{EE}, are given by the PADIE code [*Glauert and Horne*, 2005]. Only resonance with lower-band whistler mode chorus ($0.1\, f_{ce} < f < 0.5\, f_{ce}$) is considered. The presence of chorus waves is confined between $-15°$ and $15°$ magnetic latitude. The exclusion of high-latitude chorus may cause underestimation of the loss of electrons at energies >1 MeV [*Horne and Thorne*, 2003]. The diffusion coefficients are calculated as a function of L shell, energy, pitch angle, and f_{pe}/f_{ce}, the ratio of plasma frequency to the cyclotron frequency, and given by

$$\frac{f_{pe}}{f_{ce}} = \frac{1}{B}\sqrt{\frac{n_e m_e}{\varepsilon_o}} \tag{5}$$

To calculate f_{pe}/f_{ce}, which depends on the plasma density (n_e), we have embedded inside the RBE model the core plasma model of Ober and Gallagher [*Ober et al.*, 1997]. The plasma model calculates the temporal evolution of the plasma flux tube contents and equatorial plasma density distribution throughout the inner magnetosphere. The model is driven by the same magnetic and electric fields as the RBE code. The PADIE diffusion coefficients are scaled with a chorus wave intensity of 10^4 pT^2. To obtain the actual diffusion coefficients, we estimate the chorus intensity at a given location and time during the storm using the survey of CRRES plasma wave data for lower-band chorus presented by *Meredith et al.* [2001, 2003b]. For our application the wave data were binned in L shell, magnetic local time, and three levels of magnetic activity ($Kp < 2$; $2 \le Kp < 4$; $Kp \ge 4$).

[12] Equation (1) includes multiple terms of different processes. We use the method of fractional step to decompose the equation and solve only one term at a fractional step [*Fok et al.*, 1993]. To solve (1), we have to specify the electric, magnetic fields, initial distribution, and particle distribution on the nightside boundary, which is set at 10 R_E or the last closed field line. In this work, we use the Tsyganenko 2004 model [*Tsyganenko and Sitnov*, 2005] for the magnetic field and Weimer model [*Weimer*, 2001] for electric field. The electric field is updated every time step (3 s), since updating the electric field and the recalculation of the $\mathbf{E} \times \mathbf{B}$ drift are computationally fast. Updating the magnetic field, however, requires massive calculations of field line tracing and integration along field line in order to renew the particle energy and magnetic drift. The magnetic field is thus updated every 5 min. The effect of radial diffusion is integrated in these time-varying electric and magnetic fields. The NASA trapped radiation model (AE8MAX) [*Vette*, 1991; *Fung*, 1996] is used for the initial condition in the entire RBE spatial domain. The distribution at the nightside boundary is assumed to be a kappa function with density (N_{ps}) and characteristic energy (E_{ps}) modeled by linear relations with the upstream solar wind conditions [*Zheng et al.*, 2003]:

$$\begin{aligned} N_{ps}(t) &= [0.02{*}N_{sw}(t - 2\text{hr}) + 0.316]{*}\sqrt{\text{amu}} \\ E_{ps}(t) &= 0.016{*}V_{sw}(t - 2\text{hr}) - 2.4 \end{aligned} \tag{6}$$

where N_{ps} is in cm^{-3}, N_{sw} is the solar wind density in the same unit, amu is the atomic mass unit of the electron, E_{ps} is in keV, and V_{sw} is the solar wind velocity in km/s. Note that we assume a 2-h time lag between the plasma sheet condition and solar wind condition at the dayside magnetopause [*Borovsky et al.*, 1998].

[13] Figure 1 summarizes the RBE model architecture and logic. The only inputs to the model are the solar wind

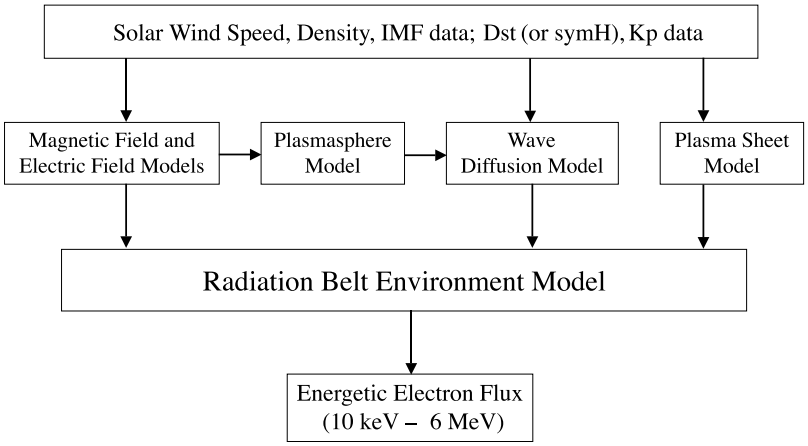

Figure 1. Model logic of the Radiation Belt Environment (RBE) model.

speed, density, and IMF and geomagnetic indices *Dst* (or *symH*) and *Kp*. The magnetic field and electric field models are driven by *Dst* or *symH*, upstream solar wind speed, density, and IMF. With the magnetic and electric fields specified, the plasmasphere model solves the core plasma density, which is used to calculate the plasma frequency needed for the PADIE code. The diffusion coefficients are then calculated for the chorus wave intensity determined by the *Kp* value. The last piece is the plasma sheet distribution, which is estimated from the solar wind density and speed (equation (6)). With all the auxiliary models in place, the RBE kinetic equation is solved to give the energetic electron fluxes at all pitch angles in the inner and the outer radiation belts.

3. Simulation of the Storm on 23–27 October 2002

[14] The storm on 23–27 October 2002 is a moderate storm with minimum *Dst* reaching −98 nT. The storm is triggered by passing of solar wind pressure pulses and southward IMF. Figure 2 plots the *Kp*, symH, solar wind density and speed, and IMF B_z, B_y measured from the ACE satellite. The temporal resolution of the ACE data is 4 min

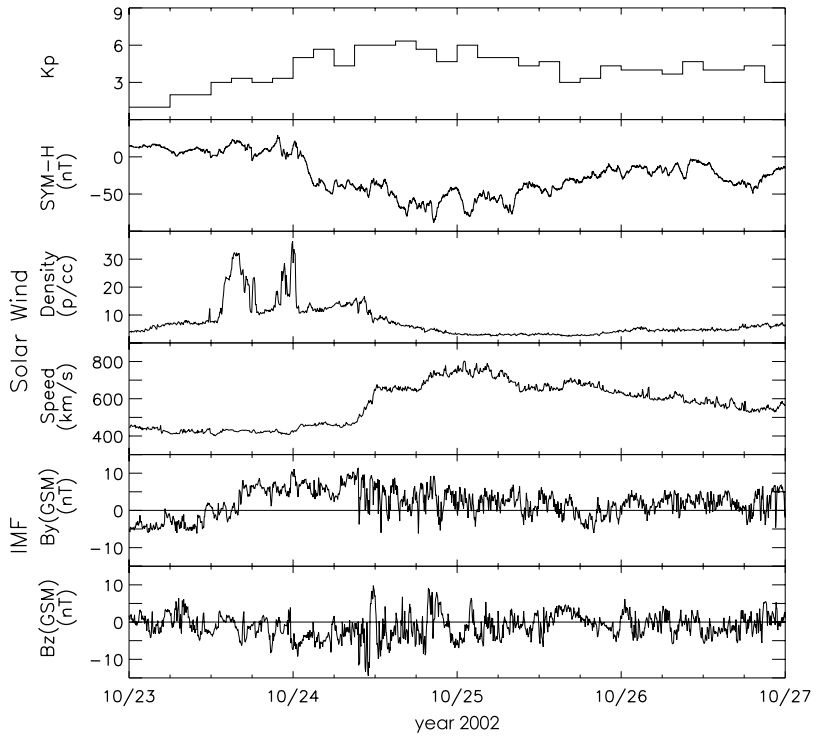

Figure 2. *Kp*, symH, solar wind density and speed, and IMF B_z, B_y measured from the ACE satellite on 23–27 October 2002. The ACE data are 44 min shifted in time.

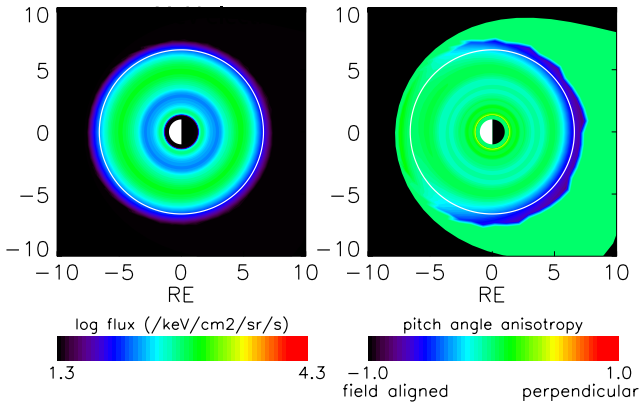

Figure 3. Simulated 0.8 MeV electron flux at the magnetic equator at quiet time, showing (left) the pitch angle averaged flux and (right) the pitch angle anisotropy. The white circles represent geosynchronous orbit.

and the data have been shifted by 44 min representing the time for solar wind to travel from the satellite to the subsolar point. The parameters plotted in Figure 2 are used to drive our magnetic (T04) and electric (Weimer 2000) field models.

[15] Figure 3 shows the simulated equatorial electron flux at 0.8 MeV during the quiet time before the storm. Figure 3 (left) is the pitch angle averaged flux and Figure 3 (right) is the pitch angle anisotropy, defined as $A = (j_\perp - j_\parallel)/(j_\perp + j_\parallel)$, where $j_\perp$ and $j_\parallel$ are perpendicular and parallel flux, respectively. $A = 0$ represents perpendicular and parallel fluxes are equal in magnitude, $A > 0$ perpendicular distribution, and $A < 0$ parallel distribution. The white circles in Figure 3 represent geosynchronous orbit. It can be seen from Figure 3 (left) that the inner and the outer belts are very well separated during quiet time. For this particular energy, the peak flux in the outer belt is located at ~4.5 R_E. In Figure 3 (right) a clear field-aligned pitch angle distribution (PAD) is seen on the nightside extending from dawn to dusk around the geosynchronous orbit. This field-aligned feature of energetic electrons and ions on the nightside has been observed [*Sibeck et al.*, 1987; *Garcia*, 1996; *Friedel et al.*, 2006] and is an effect of drift shell splitting in the asymmetric magnetic field. Particles with different pitch angles injected from the nightside drift differently to the dayside. To conserve the first adiabatic invariant, perpendicular particles tend to drift farther away from the Earth on the dayside where the magnetic field is stronger for a given radial distance. Perpendicular particles originated from the nightside geosynchronous orbit may be lost when their drift paths come across the dayside magnetopause. The drift paths of parallel particles are relatively circular and have closed drift paths around the geosynchronous orbit. As a result, more particles with field-aligned pitch angles are seen on the nightside than perpendicular particles. The strong aligned region (blue partial ring in Figure 3, right) represents the difference between the last closed orbit of field-aligned electrons and that of the perpendicular particles.

[16] The energetic electron distribution is simulated throughout the storm on 23–27 October 2002 using the RBE model. Figure 4 plots the 0.8 MeV pitch angle averaged flux at 0200 UT, 25 October at the beginning of the recovery phase, 50 h into the simulation. Figure 4 (left and middle) shows the equatorial flux and pitch angle anisotropy with the same formats as Figure 3. It can be seen that the electron flux in the inner part of the outer belt has increased by an order of magnitude during the storm. We will show later in the paper that this increase is mainly coming from electrons interacting with chorus waves. The field-aligned feature in the vicinity of the nightside geosynchronous orbit persists the whole time of the event (Figure 4, middle). On the other hand, perpendicular PADs are seen on the dayside near the magnetopause. These distinct PADs at night and day can be envisaged from the meridian view in Figure 4 (right). The white curves are field lines with equatorial crossing points at 6.6 R_E. Field-aligned distributions are characterized by lower flux at the equator than at higher latitudes along the same field line. For the field line highlighted at 0000 MLT, the equatorial flux is ~3 × 10^2 cm^{-2} s^{-1} keV^{-1} sr^{-1} (cyan) and the flux at 40° magnetic latitude is ~9 × 10^2 cm^{-2} s^{-1} keV^{-1} sr^{-1} (green), three times of the value at the equator. The perpendicular distribution near the dayside magnetopause is also seen from the relatively high flux around the equator. In the outer belt where the electron flux is high, the enhancement is dominated by perpendicular particles.

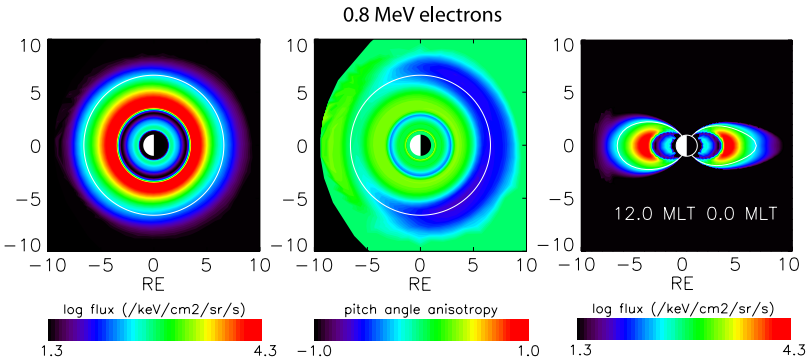

Figure 4. Simulated 0.8 MeV electron flux at the magnetic equator 50 h into the simulation at 0200 on 25 October 2002 (left, middle) in the same format as Figure 3 and (right) showing the electron flux at the noon-midnight meridian. Here, the white traces represent field lines with equatorial crossings at geosynchronous orbit.

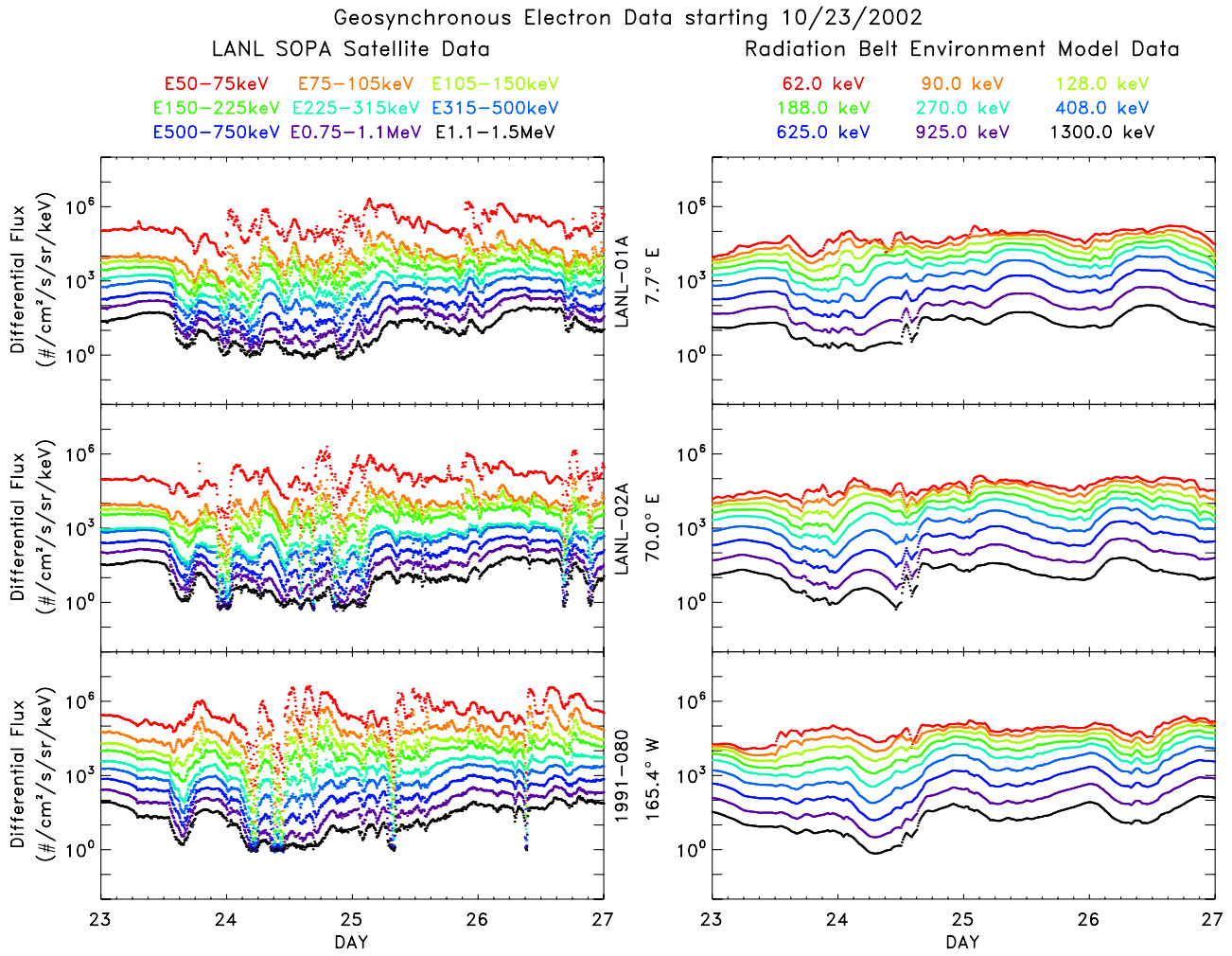

Figure 5. (left) LANL SOPA geosynchronous electron fluxes compared with (right) RBE simulated fluxes at three longitudes during the storm on 23–27 October 2002.

[17] Next we examine the storm time development of the outer belt and assess the ability of the RBE model to reproduce the observed electron flux during this event. Figure 5 (left) plots the observed electron fluxes at the geosynchronous orbits from the LANL Synchronous Orbit Particle Analyzer (SOPA) data and Figure 5 (right) plots the RBE simulated fluxes, at three geographic longitudes: 7.7°E, 70.0°E, and 165.4°W. The SOPA fluxes decrease during the storm main phase on 24 October (*Dst* effect). Electron fluxes start to recover toward the prestorm levels at late main phase. The fluctuations in the SOPA fluxes on 26 October are results of substorm activity. The simulated fluxes (Figure 5, right) exhibit similar temporal variation as those of the SOPA data, and in general the magnitudes agree very well with the data. However, the flux recovery starts earlier than the observed data, and the model fluxes lack substorm-type fluctuations.

[18] The temporal evolution of the radial profile of radiation belt particles during a storm provides important clues to identify the energization mechanisms, such as radial diffusion and wave acceleration. Figure 6 shows 2–6 MeV electron fluxes from the Proton/Electron Telescope (PET) on SAMPEX as a function of L shell and time for 23–27 October 2002 (Figure 6, top). SAMPEX orbits the Earth at 520 × 670 km altitude and 82° inclination [*Baker et al.*, 1993]. It samples magnetic field lines at the ionosphere that thread the entire radiation belts every orbit period (∼90 min). PET is a zenith-pointing solid state telescope measuring electrons from 2 to 30 MeV. These electrons are either trapped particles mirroring at SAMPEX altitudes or are precipitating into the atmosphere. The latter may be in the drift loss cone and/or the local bounce loss cone depending upon the longitudinal position of SAMPEX [*Cook et al.*, 1993]. The SAMPEX fluxes shown in Figure 6 are with orbit resolution and smoothed over 15 orbits. As shown in the figure, the outer belt, slot region, and inner belt are clearly separated in this time period. The enhancement at $L \sim 3.4$ on 23 October is a remnant from the activity taking place earlier in the month. When the storm commences on 24 October, electron fluxes start to decrease. Near the peak of the storm on late 24 October to early 25 October, electrons drift to higher L shells as a result of the ring current buildup. In the recovery phase, electron fluxes gradually increase. Flux enhancements are first seen at 3 <

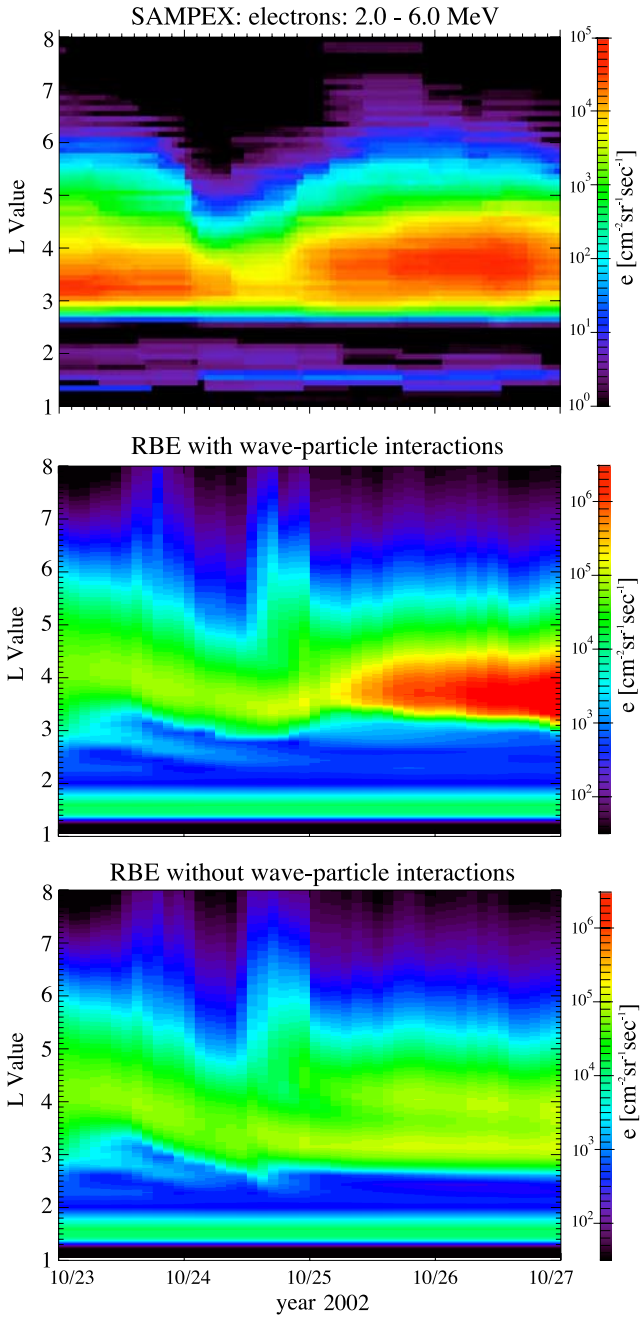

Figure 6. (top) SAMPEX 2–6 MeV electron L-time diagram during the storm on 23–27 October 2002 and RBE simulated fluxes in T04 magnetic field (middle) with and (bottom) without inclusion of wave-particle interactions, respectively.

$L < 4.5$ and then expand in both inward and outward direction.

[19] Figure 6 (middle and bottom) shows RBE simulated fluxes displayed in the same layout as the SAMPEX L-time plot. Note that the RBE data are equatorial fluxes rather than fluxes at the ionosphere as the SAMPEX data. However, as has been shown by *Kanekal et al.* [2001, 2005], the temporal variability of low-altitude fluxes measured by SAMPEX is nearly identical with the equatorial fluxes, especially during geomagnetic storms. The L values in the RBE plots are calculated by:

$$L = \frac{r_i}{\cos^2 \lambda_i} \tag{7}$$

where r_i is the ionosphere distance in R_E and λ_i is the magnetic latitude of the ionospheric foot point of the magnetic field line. The color scales of the SAMPEX and RBE data are different. The RBE fluxes are higher compared to SAMPEX since the latter observes a smaller part of the equatorial pitch angle distribution. The RBE fluxes with the inclusion of wave-particle interactions (Figure 6, middle) show similar features as the SAMPEX data. One exception is the high intensity found in the SAMPEX data on 23 October is not seen in the simulation. This is due to the fact that the RBE model uses the statistical model, AE8MAX, as initial condition and does not take into account the previous activity. When the storm hit, the flux decrease in the outer belt is also seen in the simulation. In the storm recovery, the RBE model reproduces the observed flux enhancements at about the same L shells.

[20] To identify the responsible mechanism for the flux increase, a test run is performed without the chorus wave-induced diffusions (Figure 6, bottom). Two high-flux bands are seen at around $L = 3.2$ and 4 during the storm recovery. The enhancement at $L \sim 3.2$ comes from inward radial diffusion of electrons at higher L shells. The strong flux at $L \sim 4$ is result of particle injection during the storm main phase. When wave diffusions are included (Figure 6, middle), the enhancement at the inner edge of the outer belt is diminished as a result of pitch angle diffusion loss. On the other hand, with the seed population created from particle injection, energy diffusion at $L \sim 4$ produces the flux increase in the outer belt. This enhancement cannot be explained by radial diffusion and storm injection alone. Our simulations confirm that local acceleration by wave particle interactions with whistler mode chorus can account for the flux enhancement in the center of the outer belt during the recovery phase of this storm.

[21] It is well established that strong chorus acceleration of energetic electrons takes place just outside the plasmapause where f_{pe}/f_{ce} is relatively low [*Summers et al.*, 1998; *Horne et al.*, 2006]. To demonstrate our calculation is consistent with this theory and to examine in detail how the enhancement region evolves with time, simulated 2–6 MeV electron fluxes as a function of L and time are replotted in 1-h temporal resolution (Figure 7, top). Figure 7 (middle and bottom) shows the Ober plasma density and f_{pe}/f_{ce}, respectively. Here f_{pe}/f_{ce} is plotted only for $2.5 < L < 6.5$, since this is the L range over which the wave particle interactions are introduced into the model. It can be seen that during storm recovery the values of f_{pe}/f_{ce} are low outside the plasmapause at $3 < L < 4$. This is the region of favorable chorus-electron interactions and electron fluxes start to increase at this location and time (Figure 7, top). As wave-particle interactions continue, the high-flux region extends to higher Ls and, to a less extent, to low L shells. The expansion of the flux enhancement is a result of radial diffusion since the active wave interaction region is shrinking in late recovery phase as indicated by the increasing

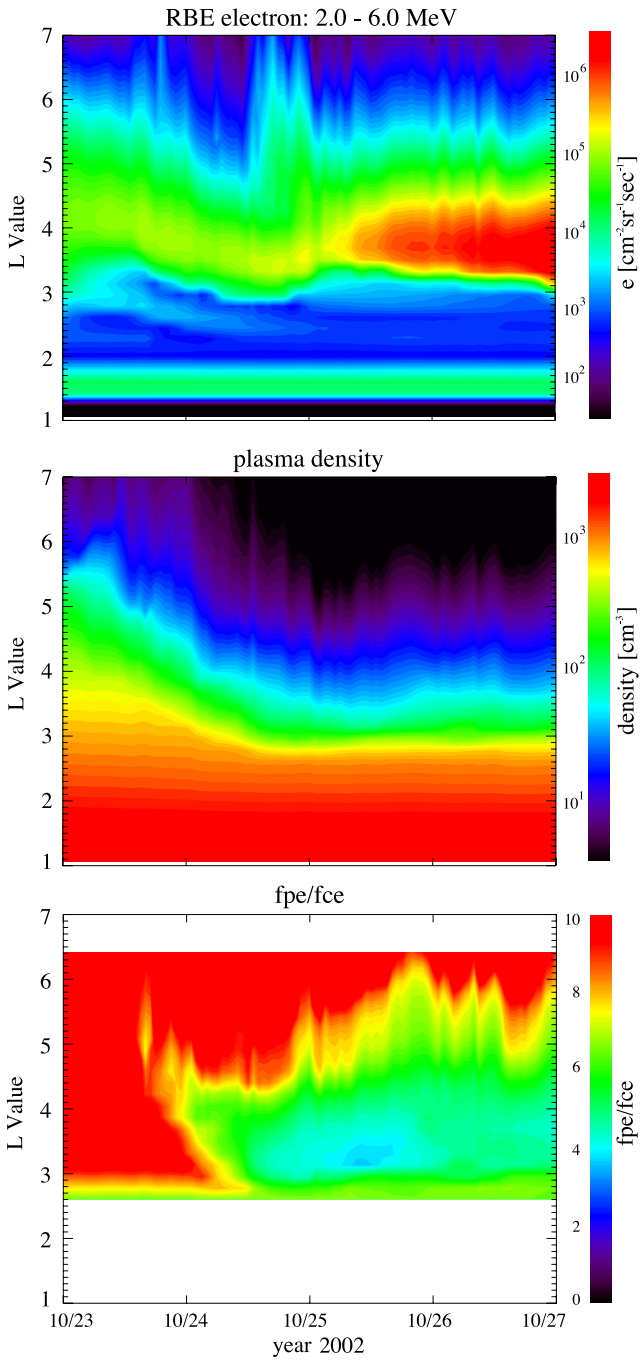

Figure 7. (top) RBE 2–6 MeV electron flux, (middle) plasmasphere density, and (bottom) $\varphi_{pe}/\varphi_{ce}$.

f_{pe}/f_{ce} ratio. *Green and Kivelson* [2004] examined the energetic electron data from POLAR/HIST instrument for acceleration event between January 1997 and January 1999. They conclude that the data is best explained by acceleration of an internal source and then outward radial diffusion to geostationary orbit. Furthermore, *Varotsou et al.* [2005] and *Horne et al.* [2006] found that local acceleration by whistler mode chorus waves followed by inward and outward radial diffusion can populate the entire radiation belt at high energies. The RBE simulation is consistent with these findings.

4. Space Weather Application

[22] As shown in Figure 1, the only inputs to the RBE model are solar wind speed, density, and the IMF, *Dst*, and *Kp* data, which are all available near real time in public Web sites. Even with increasing complexity, the RBE CPU simulation/real time ratio is close to 1 when running on a fast PC. The RBE model thus has great potential in space weather applications in providing specification of the radiation environment in geospace. A simplified version of the RBE model, using fewer grid points in M and K, is currently running in real time to provide radiation belt nowcasting updated every 15 min. The geosynchronous fluxes at longitudes of GOES-11 and 12 are extracted from the RBE real-time run and are plotted together with real-time GOES electron (>0.6 MeV) data. The model-data comparison is continually posted at http://mcf.gsfc.nasa.gov/RB_nowcast/. Figure 8 shows the RBE prediction and the GOES data for the month of December 2006. The input data to the RBE model are plotted in the bottom. The real-time version of the RBE model does not include wave-particle interactions and thus *Kp* is not one of the input parameters. As shown in Figure 8, the RBE model agrees well with the GOES data. The simulation faithfully reproduces the diurnal variation due to the offset of geographic and magnetic equators. The RBE model also closely follows the observed flux drop-off in response to decreasing *Dst*. The model performance is less exemplary during quiet conditions, where the predicted flux is usually lower than observed. Wave-induced diffusion is being implemented in the real-time version of the RBE model. We expect these additional processes will improve the prediction accuracy not only at the geosynchronous orbit but, more importantly, at the heart of the radiation belt. It should be emphasized that the measurements presented in Figure 8 are all real-time data without any selection or noise removal.

[23] The RBE model is an effective tool to predict the response of the radiation belts to adverse solar wind conditions. However, the current design allows the model to perform near real-time nowcasting only. To enhance the space weather applications of the model, it must provide hours to days of lead time in forecasting. To accomplish this goal, the RBE code must be improved to yield higher predictive accuracy. The model is then ready to be connected to a model that is able to specify the upstream solar wind conditions with sufficient lead time. Solar wind models of this kind have been established or are under development [*Fry et al.*, 2001; *Detman et al.*, 2006]. The merger of radiation belt and solar wind models represents a very worthwhile future effort in space weather applications [*Akasofu*, 2001].

5. Discussion and Conclusions

[24] In equation (1) there is no explicit description of radial diffusion transport in the RBE model. As we mentioned above, the effects of radial transport are represented by the time-varying magnetic and electric fields. Since we only update the magnetic field every 5 min, we are missing

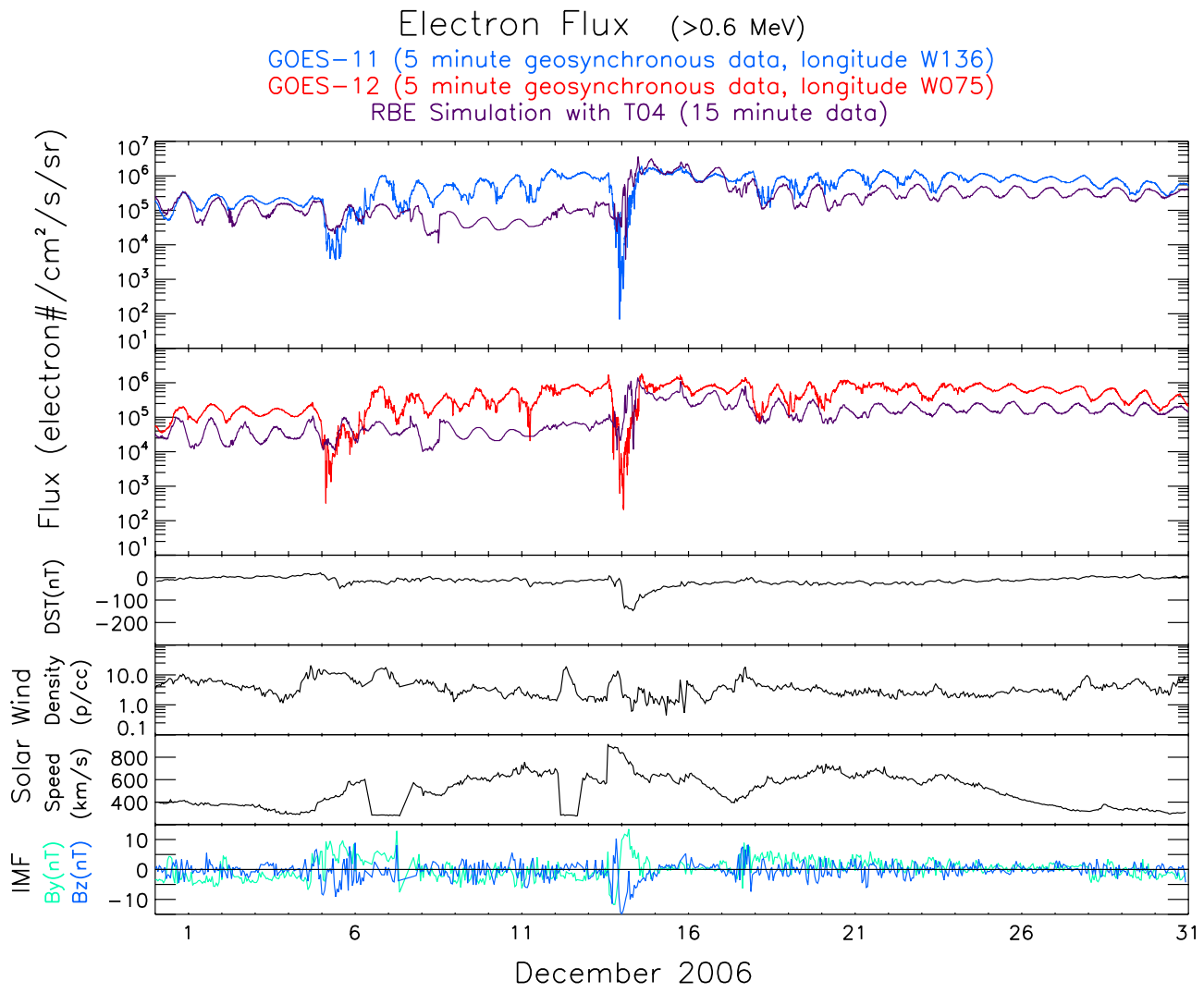

Figure 8. (top) Comparison of GOES electron fluxes (>0.6 MeV) with real-time RBE output at GOES satellite locations and (bottom) inputs to the RBE model.

the diffusive effects from the high-frequency Pc4–Pc5 fluctuations. In our previous studies [*Fok et al.*, 2001; *Zheng et al.*, 2003], we have included a radial diffusion term in the kinetic equation with diffusion coefficient given by *Cornwall* [1972]. We found, during magnetic storms, the transport due to time-varying magnetic field configuration is much larger than that from pure radial diffusion. The effect of radial diffusion may be stronger if the improved, realistic diffusion coefficients are used [i.e., *Elkington et al.*, 2003].

[25] The RBE model is sensitive to its auxiliary models: magnetic field model, electric field model, plasma sheet model, plasmasphere model, and the wave-diffusion model. Inaccuracy in these models will limit the RBE performance. A good example is the selection of the magnetic field model. It is well known that the motions of energetic ions and electrons are strongly controlled by the magnetic field configuration. To illustrate the effects of magnetic field on the RBE results, the October 2002 event is rerun using the Tsyganenko 96 (T96) model [*Tsyganenko*, 1995; *Tsyganenko and Stern*, 1996]. The T96 model does not consider the contribution from the partial ring current and the history of solar wind parameters, as all these effects are included in the T04 model. Figure 9 shows the L-time plots of the simulated electron flux in T96 magnetic field with (Figure 9, top) and without (Figure 9, bottom) chorus wave interactions. We first compare the electron fluxes calculated in the two Tsyganenko models in the absence of VLF waves. It can be seen from Figure 9 (bottom) that a flux enhancement is found at $L \sim 3.2$ during the storm recovery on 25–26 October, similar to but with lower intensity than that using the T04 model (Figure 6, bottom). Furthermore, in the T96 case, there is no noticeable enhancement at $L \sim 4$ as in the T04 case. The lower flux in the RBE-T96 run indicates that the T96 model underestimates the storm time magnetic field disturbances and thus the efficiencies of radial diffusion and particle trapping. Since the T96 model fails to provide a substantial seed population in the outer belt, including chorus associated diffusion only produces a weak enhancement there at late recovery (Figure 9, top).

[26] We have shown very good agreement between the RBE simulation results and actual SAMPEX and geosynchronous particle data. Nevertheless, more work can be done to improve the model further. Cross-diffusion in energy and pitch angle, which has been found to be

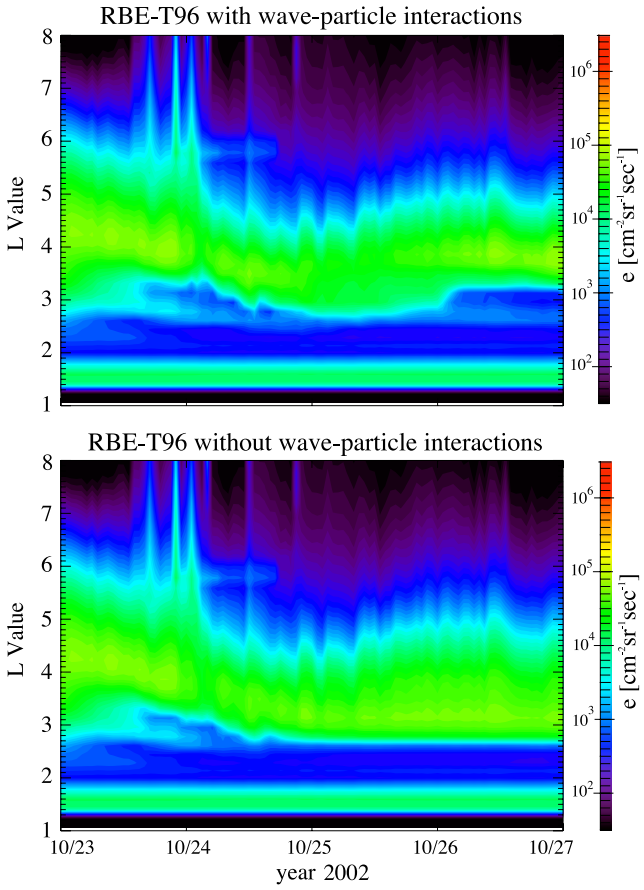

Figure 9. *L*-time diagrams of RBE simulated electron flux in T96 magnetic field with (top) and without (bottom) wave-particle interactions.

important [*Albert and Young*, 2005], has not been included in the model. Interactions with high-latitude whistler mode chorus and other waves, such as electromagnetic ion cyclotron waves and plasmaspheric hiss, should be considered as well. The diffusive effects caused by ULF waves with realistic diffusion coefficients should be reconsidered. The boundary condition of the RBE model (equation (5)) may be oversimplified and does not currently include the effects of substorm injection. All these processes will be introduced into the simulation and explored in future studies.

[27] During quiet periods, the outer belt, the slot, and the inner belt are well-defined regions. However, during intense storms, significant flux increases are seen in the slot region [e.g., *Baker et al.*, 2004] and even deep into the inner belt. The penetration distance has been found to be controlled by the strength of the storm as indicated by the *Dst* index [*Tverskaya*, 1986, 1996; *Tverskaya et al.*, 2003; *Zheng et al.*, 2006]. On the other hand, the plasmapause displaces in a similar manner. *Li et al.* [2006] found a remarkable correlation between the inner edge of the outer belt electrons and the plasmapause location. Since strong chorus acceleration of electrons takes place near the plasmapause [*Horne et al.*, 2006], the storm time erosion of the plasmasphere may place the electron acceleration zone, and thus flux enhancement, very close the Earth to the typical slot and inner belt regions. This hypothesis was tested during the Halloween storm in 2003 [*Baker et al.*, 2004]. It was shown that the enhanced flux of energetic electrons that appeared in the slot region can be explained by wave acceleration by whistler mode chorus waves [*Horne et al.*, 2005; *Shprits et al.*, 2006].

[28] As shown in section 3, simulations from the RBE model provide an explanation of the flux enhancements seen by the SAMPEX satellite during a particular storm. The RBE model will be even more relevant to the upcoming Living With a Star Radiation Belt Storm Probe (RBSP) mission, which has a low-inclination orbit and broad particle and wave measurements (NASA/TM-2002-211613). The RBE or RBE-like models will be very useful in future RBSP data analysis and interpretation. On the other hand, data from the RBSP mission can be used to probe the importance of specific physical processes in the model.

[29] In summary, a physics-based Radiation Belt Environment (RBE) model has been developed to understand the radiation belt dynamics and provide real time predictions of the radiation belt environment that can be compared with existing and new data sets. To date the findings from this model development work include:

[30] 1. In modeling the storm on 23–27 October 2002, acceleration by chorus waves is found to be responsible for electron enhancement at the center of the outer belt.

[31] 2. The RBE model is running in real time to provide nowcasting of the radiation environment. The RBE forecasting capability will be enhanced if it is connected to a solar wind forecast model.

[32] 3. Future improvements of the RBE model include adding substorm effects, considering additional wave modes and cross-diffusion.

[33] **Acknowledgments.** We like to thank Daniel Ober for providing the core plasma model. The LANL SOPA data are contributed by Geoff Reeves. SAMPEX data are provided by Shri Kanekal. Real-time GOES and ACE data are available from the NOAA Space Environment Center. Real time *Dst* data are provided by Kyoto University Geomagnetic Data Service. Thanks to Daniel Spicer, Jay Albert, Dimitris Vassiliadis, and Shing Fung for helpful suggestions and comments. The RBE real time runs were performed by Henry Lo. This research is supported by NASA Science Mission Directorate, Heliophysics Division, Living With a Star Targeted Research and Technology program, under Work Breakdown Structure 936723.02.01.01.15 and 936723.02.01.01.27.

[34] Amitava Bhattacharjee thanks T. Paul O'Brien and another reviewer for their assistance in evaluating this paper.

References

Akasofu, S.-I. (2001), Predicting geomagnetic storms as a space weather project, in *Space Weather*, *Geophys. Monogr. Ser.*, vol. 125, edited by P. Song, et al., pp. 329–337, AGU, Washington, D. C.

Albert, J. M. (1994), Quasi-linear pitch angle diffusion coefficients: Retaining high harmonics, *J. Geophys. Res.*, *99*, 23,741–23,745.

Albert, J. M., and S. L. Young (2005), Multidimensional quasi-linear diffusion of radiation belt electrons, *Geophys. Res. Lett.*, *32*, L14110, doi:10.1029/2005GL023191.

Albert, J. M., D. H. Brautigam, R. V. Hilmer, and G. P. Ginet (2001), Dynamic radiation belt modeling at the Air Force Research Laboratory, in *Space Weather*, *Geophys. Monogr. Ser.*, vol. 125, edited by P. Song, et al., pp. 281–287, AGU, Washington, D. C.

Baker, D. N. (2001), Satellite anomalies due to space storms, in *Space Storms and Space Weather Hazards*, edited by I. A. Daglis, pp. 285–311, Kluwer Acad., Boston.

Baker, D. N., G. M. Mason, O. Figueroa, G. Colon, J. G. Watzin, and R. M. Aleman (1993), An overview of the Solar, Anomalous, and Magnetospheric Particle Explorer (SAMPEX) mission, *IEEE Trans. Geosci. Remote Sens.*, *31*, 531–541.

Baker, D. N., S. G. Kanekal, X. Li, S. P. Monk, J. Goldstein, and J. L. Burch (2004), An extreme distortion of the Van Allen belt arising from the Halloween solar storm in 2003, *Nature*, *432*, 878–881.

Borovsky, J. E., M. F. Thomsen, and R. C. Elphic (1998), The driving of the plasma sheet by the solar wind, *J. Geophys. Res.*, *103*, 17,617–17,639.

Bourdarie, S., D. Boscher, T. Beutier, J.-A. Sauvaud, and M. Blanc (1997), Electron and proton radiation belt dynamic simulations during storm periods: A new asymmetric convection-diffusion model, *J. Geophys. Res.*, *102*, 17,541–17,552.

Cook, W. R., et al. (1993), PET: A proton/electron telescope for studies of magnetospheric, solar, and galactic particles, *IEEE Trans. Geosci. Remote Sens.*, *31*, 565–571.

Cornwall, J. M. (1972), Radial diffusion of ionized helium and protons: A probe for magnetospheric dynamics, *J. Geophys. Res.*, *77*, 1756–1770.

Dessler, A. J., and R. Karplus (1961), Some effects of diamagnetic ring currents on Van Allen radiation, *J. Geophys. Res.*, *66*, 2289–2295.

Detman, T., Z. Smith, M. Dryer, C. D. Fry, C. N. Arge, and V. Pizzo (2006), A hybrid heliospheric modeling system; Background solar wind, *J. Geophys. Res.*, *111*, A07102, doi:10.1029/2005JA011430.

Elkington, S. R., M. K. Hudson, and A. A. Chan (2003), Resonant acceleration and diffusion of outer zone electrons in an asymmetric geomagnetic field, *J. Geophys. Res.*, *108*(A3), 1116, doi:10.1029/2001JA009202.

Fok, M.-C., and T. E. Moore (1997), Ring current modeling in a realistic magnetic field configuration, *Geophys. Res. Lett.*, *24*, 1775–1778.

Fok, M.-C., J. U. Kozyra, A. F. Nagy, C. E. Rasmussen, and G. V. Khazanov (1993), Decay of equatorial ring current ions and associated aeronomical consequences, *J. Geophys. Res.*, *98*, 19,381–19,393.

Fok, M.-C., T. E. Moore, and M. E. Greenspan (1996), Ring current development during storm main phase, *J. Geophys. Res.*, *101*, 15,311–15,322.

Fok, M.-C., T. E. Moore, and W. N. Spjeldvik (2001), Rapid enhancement of radiation belt electron fluxes due to substorm dipolarization of the geomagnetic field, *J. Geophys. Res.*, *106*, 3873–3881.

Fok, M.-C., Y. Ebihara, T. E. Moore, D. M. Ober, and K. A. Keller (2005), Geospace storm processes coupling the ring current, radiation belt and plasmasphere, in *Inner Magnetosphere Interactions: New Perspectives from Imaging*, *Geophys. Monogr. Ser.*, vol. 159, edited by J. Burch et al., pp. 207–220, AGU, Washington, D. C.

Friedel, R. H., Y. Chen, G. D. Reeves, and T. Cayton (2006), Pitch angle evolution of energetic electrons at geosynchronous orbit during disturbed times, *Eos Trans. AGU*, *87*(52), Fall Meet. Suppl., Abstract SM41C-08.

Fry, C. D., W. Sun, C. S. Deehr, M. Dryer, Z. Smith, S.-I. Akasofu, M. Tokumaru, and M. Kojima (2001), Improvements to the HAF solar wind model for space weather predictions, *J. Geophys. Res.*, *106*, 20,985–21,001.

Fung, S. F. (1996), Recent development in the NASA trapped radiation model, in *Radiation Belts: Models and Standards*, *Geophys. Monogr. Ser.*, vol. 97, edited by J. F. Lemaire, D. Heynderickx, and D. N. Baker, pp. 79–91, AGU, Washington, D. C.

Garcia, H. A. (1996), Energetic electron pitch angle distribution parameters at 6.6 Re, as deduced from GOES X-ray observations, *Planet. Space Sci.*, *44*, 473–484.

Glauert, S. A., and R. B. Horne (2005), Calculation of pitch angle and energy diffusion coefficients with the PADIE code, *J. Geophys. Res.*, *110*, A04206, doi:10.1029/2004JA010851.

Green, J. C., and M. G. Kivelson (2004), Relativistic electrons in the outer radiation belt: Differentiating between acceleration mechanisms, *J. Geophys. Res.*, *109*, A03213, doi:10.1029/2003JA010153.

Green, J. C., T. G. Onsager, T. P. O'Brien, and D. N. Baker (2004), Testing loss mechanisms capable of rapidly depleting relativistic electron flux in the Earth's outer radiation belt, *J. Geophys. Res.*, *109*, A12211, doi:10.1029/2004JA010579.

Horne, R. B. (2002), The contribution of wave particle interactions to electron loss and acceleration in the Earth's radiation belts during geomagnetic storms, in *Review of Radio Science 1999–2002*, edited by W. R. Stone, chap. 33, pp. 801–828, IEEE Press, Piscataway, N. J.

Horne, R. B., and R. M. Thorne (1998), Potential waves for relativistic electron scattering and stochastic acceleration during magnetic storms, *Geophys. Res. Lett.*, *25*, 3011–3014.

Horne, R. B., and R. M. Thorne (2003), Relativistic electron acceleration and precipitation during resonant interactions with whistler-mode chorus, *Geophys. Res. Lett.*, *30*(10), 1527, doi:10.1029/2003GL016973.

Horne, R. B., R. M. Thorne, S. A. Glauert, J. M. Albert, N. P. Meredith, and R. R. Anderson (2005a), Timescale for radiation belt electron acceleration by whistler mode chorus waves, *J. Geophys. Res.*, *110*, A03225, doi:10.1029/2004JA010811.

Horne, R. B., et al. (2005b), Wave acceleration of electrons in the Van Allen radiation belts, *Nature*, *437*, 227, doi:10.1038/nature03939.

Horne, R. B., N. P. Meredith, S. A. Glauert, A. Varotsou, D. Boscher, R. M. Thorne, Y. Y. Shprits, and R. R. Anderson (2006), Mechanisms for the acceleration of radiation belt electrons, in *Recurrent Magnetic Storms: Corotating Solar Wind Streams*, *Geophys. Monogr. Ser.*, vol. 167, edited by B. T. Tsurutani et al., pp. 151–173, AGU, Washington, D. C.

Hudson, M. K., S. R. Elkington, J. G. Lyon, V. A. Marchenko, I. Roth, M. Temerin, and M. S. Gussenhoven (1996), MHD/particle simulations of radiation belt formation during a storm sudden commencement, in *Radiation Belts: Models and Standards*, *Geophys. Monogr. Ser.*, vol. 97, edited by J. F. Lemaire, D. Heynderickx, and D. N. Baker, pp. 57–62, AGU, Washington, D. C.

Iles, R. H. A., A. N. Fazakerley, A. D. Johnstone, N. P. Meredith, and P. Buhler (2002), The relativistic electron response in the outer radiation belt during magnetic storms, *Ann. Geophys.*, *20*, 957–965.

Kanekal, S. G., D. N. Baker, and J. B. Blake (2001), Multisatellite measurements of relativistic electron: Global coherence, *J. Geophys. Res.*, *106*, 29,721–29,732.

Kanekal, S. G., R. Friedel, G. D. Reeves, D. N. Baker, and J. B. Blake (2005), Relativistic electron events in 2002: Studies of pitch angle isotropization, *J. Geophys. Res.*, *110*, A12224, doi:10.1029/2004JA010974.

Kim, H.-J., and A. A. Chan (1997), Fully relativistic changes in storm time relativistic electron fluxes, *J. Geophys. Res.*, *102*, 22,107–22,116.

Li, X., I. Roth, M. Temerin, J. Wygant, M. K. Hudson, and J. B. Blake (1993), Simulation of the prompt energization and transport of radiation particles during the March 23, 1991, SSC, *Geophys. Res. Lett.*, *20*, 2423–2426.

Li, X., M. Temerin, D. N. Baker, G. D. Reeves, and D. Larson (2001), Quantitative prediction of radiation belt electrons at geostationary orbit based on solar wind measurements, *Geophys. Res. Lett.*, *28*, 1887–1890.

Li, X., D. N. Baker, T. P. O'Brien, L. Xie, and Q. G. Zong (2006), Correlation between the inner edge of outer radiation belt electrons and the innermost plasmapause location, *Geophys. Res. Lett.*, *33*, L14107, doi:10.1029/2006GL026294.

Lyons, L. R., R. M. Thorne, and C. F. Kennel (1972), Pitch-angle diffusion of radiation belt electrons with the plasmasphere, *J. Geophys. Res.*, *77*, 3455–3474.

Meredith, P. N., R. B. Horne, and R. R. Anderson (2001), Substorm dependence of chorus amplitudes: Implications for the acceleration of electrons to relativistic energy, *J. Geophys. Res.*, *106*, 13,165–13,178.

Meredith, N. P., R. B. Horne, R. H. A. Iles, R. M. Thorne, D. Heynderickx, and R. R. Anderson (2002), Outer zone relativistic electron acceleration associated with substorm-enhanced whistler-mode chorus, *J. Geophys. Res.*, *107*(A7), 1144, doi:10.1029/2001JA900146.

Meredith, N. P., M. Cain, R. B. Horne, R. M. Thorne, D. Summers, and R. R. Anderson (2003a), Evidence for chorus-driven electron acceleration to relativistic energies from a survey of geomagnetically disturbed periods, *J. Geophys. Res.*, *108*(A6), 1248, doi:10.1029/2002JA009764.

Meredith, P. N., R. B. Horne, R. M. Thorne, and R. R. Anderson (2003b), Favored regions for chorus-driven electron acceleration to relativistic energies in the Earth's outer radiation belt, *Geophys. Res. Lett.*, *30*(16), 1871, doi:10.1029/2003GL017698.

Meredith, N. P., R. B. Horne, S. A. Glauert, and R. R. Anderson (2007), Slot region electron loss timescales due to plasmaspheric hiss and lightning generated whistlers, *J. Geophys. Res.*, *112*, A08214, doi:10.1029/2007JA012413.

Miyoshi, Y., A. Morioka, T. Obara, H. Misawa, T. Nagai, and Y. Kasahara (2003), Rebuilding process of the outer radiation belt during the November 3, 1993, magnetic storm: NOAA and EXOS-D observations, *J. Geophys. Res.*, *108*(A1), 1004, doi:10.1029/2001JA007542.

Miyoshi, Y. S., V. K. Jordanova, A. Morioka, M. F. Thomsen, G. D. Reeves, D. S. Evans, and J. C. Green (2006), Observations and modeling of energetic electron dynamics during the October 2001 storm, *J. Geophys. Res.*, *111*, A11S02, doi:10.1029/2005JA011351.

Ober, D. M., J. L. Horwitz, and D. L. Gallagher (1997), Formation of density troughs embedded in the outer plasmasphere by subauroral ion drift events, *J. Geophys. Res.*, *102*, 14,595–14,602.

Paulikas, G. A., and J. B. Blake (1979), Effects of the solar wind on magnetospheric dynamics: Energetic electrons at the synchronous orbit, in *Quantitative Modeling of Magnetospheric Processes*, *Geophys. Monogr. Ser.*, vol. 21, edited by W.-P. Olsen, pp. 180–202, AGU, Washington, D. C.

Reeves, G. D., K. L. McAdams, and R. H. W. Friedel (2003), Acceleration and loss of relativistic electrons during geomagnetic storms, *Geophys. Res. Lett.*, *30*(10), 1529, doi:10.1029/2002GL016513.

Schulz, M., and L. J. Lanzerotti (1974), *Particle Diffusion in the Radiation Belts*, *Phys. and Chem. in Space*, vol. 7, Springer, New York.

Shprits, Y. Y., R. M. Thorne, R. B. Horne, S. A. Glauert, M. Cartwright, C. T. Russel, D. N. Baker, and S. G. Kanekal (2006), Acceleration mechanism responsible for the formation of the new radiation belt during the 2003 Halloween solar storms, *Geophys. Res. Lett.*, *33*, L05104, doi:10.1029/2005GL024256.

Sibeck, D. G., R. W. McEntire, A. T. Y. Lui, R. E. Lopez, and S. M. Krimigis (1987), Magnetic field drift shell splitting: Cause of unusual dayside particle pitch angle distributions during storms and substorms, *J. Geophys. Res.*, *92*, 13,485–13,497.

Summers, D., and C. Ma (2000), A model for generating relativistic electrons in the Earth's inner magnetosphere based on gyroresonant wave-particle interactions, *J. Geophys. Res.*, *105*, 2625–2640.

Summers, D., R. M. Thorne, and F. Xiao (1998), Relativistic theory of wave-particle resonant diffusion with application to electron acceleration in the magnetosphere, *J. Geophys. Res.*, *103*, 20,487–20,500.

Summers, D., B. Ni, and N. P. Meredith (2007), Timescales for radiation belt electron acceleration and loss due to resonant wave particle interactions: 2. Evaluation for VLF chorus, ELF hiss, and EMIC waves, *J. Geophys. Res.*, *112*, A04207, doi:10.1029/2006JA011993.

Thorne, R. M., R. B. Horne, S. A. Glauert, N. P. Meredith, Y. Y. Shprits, D. Summers, and R. R. Anderson (2005), The influence of wave-particle interactions on relativistic electrons during storms, in *Inner Magnetosphere Interactions: New Perspectives From Imaging*, *Geophys. Monogr. Ser.*, vol. 159, edited by J. Burch, M. Schulz, and H. Spence, AGU, Washington, D. C.

Tsyganenko, N. A. (1995), Modeling the Earth's magnetospheric magnetic field confined within a realistic magnetopause, *J. Geophys. Res.*, *100*, 5599–5612.

Tsyganenko, N. A., and M. I. Sitnov (2005), Modeling the dynamics of the inner magnetosphere during strong geomagnetic storms, *J. Geophys. Res.*, *110*, A03208, doi:10.1029/2004JA010798.

Tsyganenko, N. A., and D. P. Stern (1996), Modeling the global magnetic field of the large-scale Birkeland current systems, *J. Geophys. Res.*, *101*, 27,187–27,198.

Tverskaya, L. V. (1986), Electron-injection boundary in the Earth's magnetosphere, *Geomagn. Aeron.*, *26*, 736–737.

Tverskaya, L. V. (1996), The latitude position dependence of the relativistic electron maximum as a function of Dst, *Adv. Space Res.*, *18*, 135.

Tverskaya, L. V., N. N. Pavlov, J. B. Blake, R. S. Selesnick, and J. F. Fennell (2003), Predicting the L-position of the storm-injected relativistic electron belt, *Adv. Space Res.*, *31*, 1039–1044.

Ukhorskiy, A. Y., B. J. Anderson, P. C. Brandt, and N. A. Tsyganenko (2006), Storm time evolution of the outer radiation belt: Transport and losses, *J. Geophys. Res.*, *111*, A11S03, doi:10.1029/2006JA011690.

Varotsou, A., D. Boscher, S. Bourdarie, R. B. Horne, S. A. Glauert, and N. P. Meredith (2005), Simulation of the outer radiation belt electrons near geosynchronous orbit including both radial diffusion and resonant interaction with whistler mode chorus waves, *Geophys. Res. Lett.*, *32*, L19106, doi:10.1029/2005GL023282.

Vette, J. I. (1991), The AE-8 trapped electron model environment, *NSSDC/WDC-A-R&S 91-24*, NASA Goddard Space Flight Cent., Greenbelt, Md.

Weimer, D. R. (2001), An improved model of ionospheric electric potentials including substorm perturbations and applications to the Geospace Environment Modeling November 24, 1996, event, *J. Geophys. Res.*, *106*, 407–416.

Zheng, Y., M.-C. Fok, and G. V. Khazanov (2003), A radiation belt-ring current forecasting model, *Space Weather*, *1*(3), 1013, doi:10.1029/2003SW000007.

Zheng, Y., A. T. Y. Lui, X. Li, and M.-C. Fok (2006), Characteristics of 2–6 MeV electrons in the slot region and inner radiation belt, *J. Geophys. Res.*, *111*, A10204, doi:10.1029/2006JA011748.

M.-C. Fok, Geospace Physics Laboratory, NASA Goddard Space Flight Center, Code 673, Greenbelt, MD 20771, USA. (mei-ching.h.fok@nasa.gov)

S. A. Glauert, R. B. Horne, and N. P. Meredith, Physical Science Division, British Antarctic Survey, High Cross, Madingley Road, Cambridge CB3 0ET, UK.